Draft version May 4, 2021
Typeset using LaTeX **twocolumn** style in AASTeX63

Accessing Intermediate-Mass Black Holes in 728 Globular Star Clusters in NGC 4472

J. M. Wrobel,[1] T. J. Maccarone,[2] J. C. A. Miller-Jones,[3] and K. E. Nyland[4]

[1] *National Radio Astronomy Observatory, P.O. Box O, Socorro, NM 87801, USA*
[2] *Department of Physics and Astronomy, Texas Tech University, Box 41051, Lubbock, TX 79409-1051, USA*
[3] *International Centre for Radio Astronomy Research, Curtin University, GPO Box U1987, Perth, WA 6845, Australia*
[4] *National Research Council, Resident at the U.S. Naval Research Laboratory, 4555 Overlook Avenue SW, Washington, DC 20375, USA*

(Received as ngVLA Memo # 87)

ABSTRACT

Intermediate-mass black holes (IMBHs) by definition have masses of $M_{\rm IMBH} \sim 10^{2-5}\ M_\odot$, a range with few observational constraints. Finding IMBHs in globular star clusters (GCs) would validate a formation channel for massive black-hole seeds in the early universe. Here, we simulate a 60-hour observation with the next-generation Very Large Array (ngVLA) of 728 GC candidates in the Virgo Cluster galaxy NGC 4472. Interpreting the radio detection thresholds as signatures of accretion onto IMBHs, we benchmark IMBH mass thresholds in three scenarios and find the following: (1) Radio analogs of ESO 243-49 HLX-1, a strong IMBH candidate with $M^{\rm HLX}_{\rm IMBH} \sim 10^{4-5}\ M_\odot$ in a star cluster, are easy to access in all 728 GC candidates. (2) For the 30 GC candidates with extant X-ray detections, the empirical fundamental-plane relation involving black hole mass plus X-ray and radio luminosities suggests access to $M^{\rm FP}_{\rm IMBH} \sim 10^{1.7-3.6}\ M_\odot$, with an uncertainty of 0.44 dex. (3) A fiducial Bondi accretion model was applied to all 728 GC candidates and to radio stacks of GC candidates. This model suggests access to IMBH masses, uncertain by 0.39 dex, of $M^{\rm B}_{\rm IMBH} \sim 10^{4.9-5.1}\ M_\odot$ for individual GC candidates and $M^{\rm B,stack}_{\rm IMBH} \sim 10^{4.5}\ M_\odot$ for radio stacks of about 100-200 GC candidates. The Bondi model offers initial guidance, but it should be superceeded by hydrodynamical simulations of gas flows in GCs.

Keywords: Intermediate-mass black holes (816); Globular star clusters (656); Accretion (14)

1. MOTIVATION

By definition, intermediate-mass black holes (IMBHs) have masses of $M_{\rm IMBH} \sim 10^2 - 10^5\ M_\odot$. Discovering them in present-day globular star clusters (GCs) would validate a formation channel for the seeds of massive black holes (BHs) in the early universe (for a review, see Greene et al. 2020). It would also inform predictions for gravitational wave and tidal disruption events offset from galactic nuclei (e.g., Fragione et al. 2018).

To search for IMBHs in GCs, one looks for evidence that the IMBHs are influencing the properties of their GC hosts. Within the Local Group, a common approach is to scrutinize optical or infrared data for the dynamical signatures of IMBHs on the orbits of stars in the GCs. Further afield, the extremely large telescopes in the 30m class aim to measure, at a distance of 10 Mpc, an IMBH mass of $10^5\ M_\odot$ by spatially resolving its sphere of influence in its GC host (Do et al. 2014). Such sphere-of-influence searches are susceptible to measuring high concentrations of stellar remnants rather than an IMBH (e.g., Anderson & van der Marel 2010; van der Marel & Anderson 2010; Baumgardt 2017; Rui et al. 2021). It is thus important to develop alternate ways to search for IMBHs in GCs.

One alternate approach, first suggested by Maccarone (2004), builds on extensive studies of accretion signatures from stellar-mass and supermassive BHs. By analogy with stellar-mass BHs (reviewed by Fender & Belloni 2012), it is expected that an IMBH will spend more time in the hard X-ray state - including quiesence - than in the soft X-ray state. In the typical case of just a few radio observations, it is likely that they will sample the steady radio emission characterizing the hard X-ray state, rather than the flaring radio emssion occuring

Corresponding author: J. M. Wrobel
jwrobel@nrao.edu

during a transition from the hard X-ray state to the soft X-ray state. These concepts lead to the following three scenarios:

- Seek radio emission resembling that from ESO 243-49 HLX-1 in its hard X-ray state. HLX-1 is a strong IMBH candidate in a star cluster which may have a GC-like stellar mass (Farrell et al. 2009; Soria et al. 2012, 2017; Cseh et al. 2015).
- Use the empirical fundamental-plane regression for the hard X-ray state, plus observations of X-ray and radio luminosities, to estimate an IMBH mass (Merloni et al. 2003; Falke et al. 2004; Plotkin et al. 2012; Miller-Jones et al. 2012).
- Use a fiducial, semi-empirical model to predict the mass of an IMBH that, if experiencing Bondi accretion in the hard X-ray state, would be consistent with the observed radio luminosity (Maccarone & Servillat 2008, 2010; Strader et al. 2012).

It is expected that the radio continuum emission from an IMBH will be persistent over time, flat-spectrum, jet-like but spatially unresolved at the anticipated resolutions, and located at or close to the dynamical center of the GC (Maccarone 2004). Where necesary, we adopt a radio spectral index of zero when evaluating radio luminosities or comparing observations at different wavelengths.

Evolutionary models of GCs predict that only a few percent overall will retain their putative IMBHs against gravitational wave recoils (e.g., Holley-Bockelmann et al. 2008; Fragione et al. 2018). Examining a large number of GCs per galaxy is thus key, driving us to consider massive, bulge-dominated galaxies (Harris et al. 2013). Section 2 describes how we select a galaxy and simulate a radio observation of it. In Section 3 we quantify the radio detection thresholds, interpret them as signatures of accretion onto IMBHs, and benchmark the associated IMBH mass thresholds within the context of the scenarios above. We close in Section 4 with a summary and conclusions.

2. SIMULATED OBSERVATION

Some massive, bulge-dominated galaxies exhibit strong radio continuum emission (Nagar et al. 2005; Nyland et al. 2016), potentially limiting the depths of radio searches. We avoid M87 and other such galaxies, and focus on NGC 4472, at a distance of 16.7 Mpc and the optically brightest galaxy in the Virgo Cluster (Blakeslee et al. 2009). Ground-based imaging of NGC 4472 over tens of arcminutes suggests that the total number of GCs is about 9000, with their surface density peaking in the innermost few arcminutes (Durrell et al. 2014). Here we focus on that innermost region of NGC 4472 and adopt the Maccarone et al. (2003) catalog of GC candidates derived from deep HST/WFPC2 photometry in V(F555W) and I(F814W) bands. We simulate an observation of those candidates with the next-generation Very Large Array (ngVLA; Selina et al. 2018).

A typical GC has a half-starlight diameter of 5 pc (Brodie & Strader 2006), which subtends 60 mas at NGC 4472's distance. We thus select a wavelength of 2cm to ensure an adequately fine spatial resolution of 100 mas (8.1 pc) and an adequately large field of view (FoV) to encompass hundreds of GC candidates in one ngVLA pointing. Balancing loss of sensitivity due to primary beam attenuation against the number of GC candidates, we adopt a FoV of 5.09 arcmin (24.7 kpc) set by the primary beam at full width at quarter maximum (FWQM).

GC candidates were identified via their size and color (Maccarone et al. 2003). We estimate the stellar masses $M_\star$ of the GC candidates from the I-band photometry, assuming a Solar value of 4.52 AB mag (Willmer 2018) and a mass-to-light ratio of 1.4 (Jordan et al. 2007). After excluding one GC candidate as likely being too massive for a bona fide GC (Norris et al. 2019), we are left with 728 GC candidates in a single ngVLA pointing (Figure 1). As yet, there is no information as to which GC candidates are core-collapsed and which are not. The consensus of theoretical studies is that core-collapsed GCs cannot harbour IMBHs (Rui et al. 2021, and references therein). The ngVLA pointing will encompass both types.

We then pick a reasonable observation duration on NGC 4472 of 60 hours. Using the ngVLA Sensitivity Calculator (https://gitlab.nrao.edu/vrosero/ngvla-sensitivity-calculator), the Main Array of 214 18-m antennas at a wavelength of 2cm will provide a detection threshold of $S_{2\mathrm{cm}} = 3 \times 0.034$ μJy beam^{-1} at 3σ at the peak of the primary beam. NGC 4472 hosts a low-luminosity AGN with a peak 2cm flux density of 3.7 mJy for an angular resolution of 150 mas (Nagar et al. 2005). Imaging NGC 4472 with the ngVLA will thus require a dynamic range of about $(3700/0.034) \sim 10^5$, achievable based on the facility's planned performance (Selina et al. 2018). As Nyland et al. (2018) emphasize, those contemplating deep ngVLA searches – as simulated here – should be aware that sky regions containing only a few mJy can start to suffer from dynamic-range limitations.

3. IMPLICATIONS

3.1. *Radio Luminosity Thresholds*

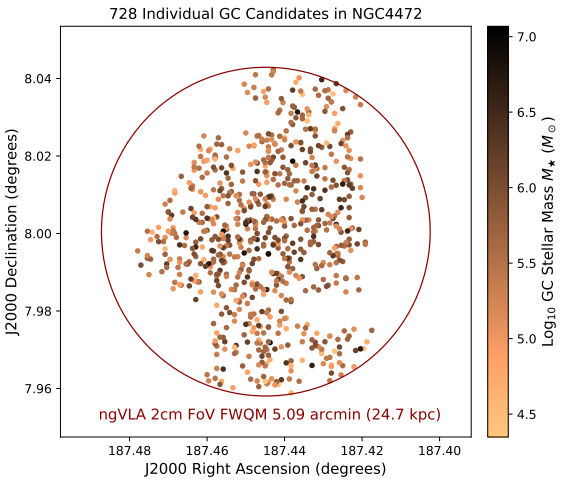

Figure 1. Locations of 728 individual GC candidates in NGC 4472 (Maccarone et al. 2003) and within a FoV equal to FWQM of the primary beam of an ngVLA antenna at a wavelength of 2cm (Selina et al. 2018). The color gradation conveys estimates of the stellar masses $M_\star$ of the GC candidates.

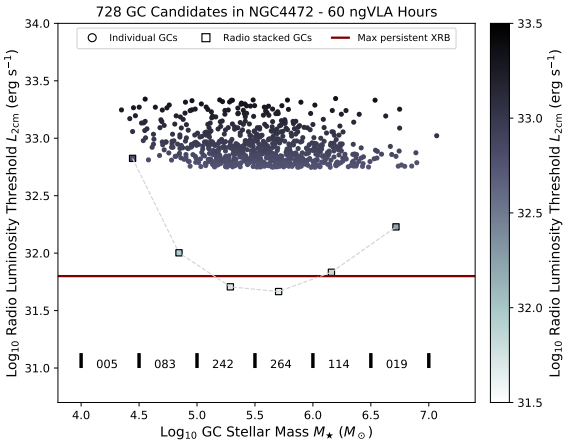

Figure 2. Radio luminosity thresholds $L_{2\rm cm}$ at 3σ from a simulated ngVLA observation of GC candidates in NGC 4472, versus the stellar masses $M_\star$ of the GC candidates. The color gradation encodes the radio luminosity thresholds. The circles mark 728 individual GC candidates (Maccarone et al. 2003). The spread in $L_{2\rm cm}$ arises from the primary beam attenuation at the locations of the GC candidates. The numbers of GC candidates in bins of width 0.5 dex in stellar mass $M_\star$ are noted. The squares mark the radio luminosity thresholds $L_{2\rm cm}^{\rm stack}$ after stacking the GC candidates in each of the bins. The horizontal line shows the maximum persistent luminosity of stellar-mass XRBs (Bahramian et al. 2020).

At the location of each GC candidate, we correct the radio detection threshold for the primary beam attenuation at 2cm and then convert the corrected detection threshold to a radio luminosity threshold $L_{2\rm cm}$ at NGC 4472's distance. As Figure 2 demonstrates, the radio luminosity thresholds reach $L_{2\rm cm} \sim 10^{32.7-33.3}$ erg s^{-1}.

To explore the prospects for deeper detections, we also wish to stack the corrected radio detection thresholds of GC candidates with similar stellar masses. Techniques for stacking extragalactic GC populations have been developed using VLA images of nearby galaxies (Wrobel et al. 2015, 2016; Wrobel & Nyland 2020). Here, we opt to segregate NGC 4472's individual GC candidates into bins of width 0.5 dex in stellar mass $M_\star$. For each bin, we evaluate its number of GC candidates, median $M_\star^{\rm stack}$, weighted-mean detection threshold $S_{2\rm cm}^{\rm stack}$, and associated radio luminosity threshold $L_{2\rm cm}^{\rm stack}$ (Table 1). We caution that such stacking implicitly assumes a high occupation fraction of IMBHs in each bin's GCs. Meeting this condition might be easier in the high-stellar-mass bins: GC evolutionary models suggest that the more massive a GC, the more likely it is to retain a putative IMBH against gravitational wave recoils (e.g., Holley-Bockelmann et al. 2008; Fragione et al. 2018).

Regarding possible radio contaminants behind NGC 4472's GC candidates, simulated source counts near 2cm suggest that star forming galaxies will dominate at μJy levels (Wilman et al. 2008). As such galaxies have steep specta and finite sizes, they will not be mistaken for IMBHs that have flat spectra and are point-like.

Regarding possible radio contaminants within NGC 4472's GC candidates, studies of stellar-mass X-ray binaries (XRBs) in the Milky Way show that their persistent radio luminosities at 6cm top out at about $10^{31.3}$ erg s^{-1} for BH systems (Bahramian et al. 2020). Scaling a flat-spectrum contaminant from 6cm to 2cm in an individual GC, this translates to a radio luminosity $L_{2\rm cm} \sim 10^{31.8}$ erg s^{-1}, well below the radio luminosity thresholds of individual GC candidates in NGC 4472 (Figure 2). If every GC harboured such an extreme contaminant, a signal could just emerge above the deepest stacked thresholds $L_{2\rm cm}^{\rm stack}$ (Figure 2, Table 1); we dismiss such a contrived situation. Also, one radio-flaring XRB in an ultraluminous state has been identified in M31 (Middleton et al. 2013); while a radio analog of it could be detected in NGC 4472, it would fade after a few months so not be mistaken for the persistent emitters that we seek.

3.2. *X-ray Detections*

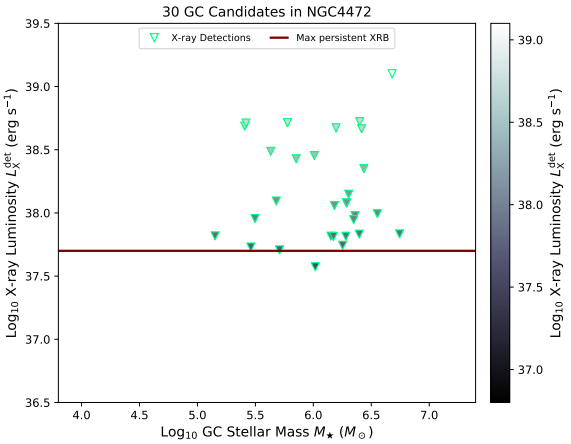

Figure 3. X-ray luminosities $L_{\rm X}^{\rm det}$ of 30 Chandra-detected GC candidates in NGC 4472 (Maccarone et al. 2003) versus their stellar masses $M_\star$. The color gradation encodes the X-ray luminosities. The horizontal line shows the maximum persistent luminosity of stellar-mass X-ray binaries (Maccarone et al. 2003).

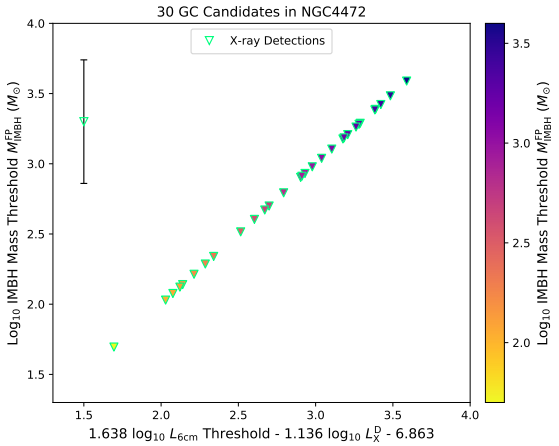

Figure 4. IMBH mass thresholds suggested from the fundamental plane, $M_{\rm IMBH}^{\rm FP}$, for the simulated ngVLA observation of 30 GC candidates in NGC 4472 with Chandra detections (Maccarone et al. 2003). The color gradation encodes $M_{\rm IMBH}^{\rm FP}$ and the example error bar shows its 0.44 dex uncertainty (Miller-Jones et al. 2012).

Only 30 of the 728 GC candidates, or 4%, have been detected with Chandra (Maccarone et al. 2003). Their X-ray luminosities $L_{\rm X}^{\rm det}$ are shown in Figure 3 after being adjusted to our assumed distance for NGC 4472. If these 30 detections arise from BH XRBs, their luminosities would correspond to systems in their high/soft state or very high state. However, the signal-to-noise of the X-ray spectroscopy was insufficient to establish the emission states. Here, we assume that the 30 detections arise from BHs of unspecified mass that are emitting in the hard X-ray state. If improved X-ray spectroscopy eventually excludes hard-state emission, the $L_{\rm X}^{\rm det}$ values should be treated as upper limits on any hard-state emission.

3.3. *Analogs of ESO 243-49 HLX-1*

ESO 243-49 HLX-1 is a strong IMBH candidate, of mass $M_{\rm IMBH}^{\rm HLX} \sim 10^{4-5}\ M_\odot$, in a star cluster which may have a GC-like stellar mass (Farrell et al. 2009; Soria et al. 2012, 2017). For a luminosity distance of 92 Mpc, HLX-1 is expected to have a steady 2cm luminosity of $L_{\rm 2cm} \sim 10^{36.6}$ erg s^{-1} while in its hard X-ray state (Cseh et al. 2015). If that steady emission is being Doppler boosted by a factor of about five to ten, as Cseh et al. (2015) argue, then its side-on luminosity would be about $L_{\rm 2cm} \sim 10^{35.6-35.8}$ erg s^{-1}. Given these various radio luminosities, Figure 2 makes it clear that radio analogs of HLX-1 would be easy to access among NGC 4472's 728 GC candidates.

Figure 3 shows that none of NGC 4472's GC candidates has an observed X-ray luminosity (Maccarone et al. 2003) as high as that of HLX-1 in its hard state, $L_{\rm X} \sim 10^{40.3}$ erg s^{-1} (Godet et al. 2012). This absence of X-ray analogs of HLX-1 would be consistent with an absence of radio analogs of HLX-1, discussed above. However, the radio luminosity thresholds would be more than two orders of magnitude lower than even a deboosted version of HLX-1. This would enable searches for less radio-extreme sources, even in the case where their X-ray counterparts were heavily absorbed, such that their X-ray emission was not especially remarkable.

3.4. *IMBH Masses and the Fundamental Plane*

Figure 3 shows the X-ray luminosities $L_{\rm X}^{\rm det}$ for 30 GC candidates in NGC 4472 (Maccarone et al. 2003). As Section 3.2 mentions, we assume that those 30 X-ray detections arise from BHs of unspecified mass that are emitting in the hard X-ray state. Radio luminosity thresholds $L_{\rm 2cm}$ are also available from Figure 2 for those 30 GC candidates.

Armed with this information for the 30 GC candidates, we can invoke the empirical fundamental-plane (FP) relation for the hard X-ray state to estimate their IMBH mass thresholds $M_{\rm IMBH}^{\rm FP}$, with an uncertainty of 0.44 dex (Miller-Jones et al. 2012). That FP relation adopts an X-ray range of 0.5-10 keV and a radio wavelength of 6cm. The $L_{\rm X}^{\rm det}$ values from Maccarone et al. (2003) cover 0.5-8 keV which, at the signal-to-noise ratios involved, is a suitable proxy for the FP's range. The $L_{\rm 2cm}$ thresholds from Figure 2 were scaled to $L_{\rm 6cm}$ assuming a flat radio spectrum. While other FP studies (e.g., Gultekin et al. 2019) suggest larger uncertain-

ties than those advocated by Miller-Jones et al. (2012), we follow Miller-Jones et al. (2012) for consistency with our earlier work on Milky Way GCs (Maccarone 2004; Strader et al. 2012) and extragalactic GCs (Wrobel et al. 2015, 2016, 2018; Wrobel & Nyland 2020).

The FP results are shown in Figure 4. They demonstrate that measurements of $L_{\rm X}^{\rm det}$ and thresholds for $L_{\rm 6cm}$ provide access to IMBH mass thresholds of $M_{\rm IMBH}^{\rm FP} \sim 10^{1.7-3.6}\ M_\odot$. Notably, among previous attempts to apply the FP to extragalactic GCs (Miller-Jones et al. 2012; Wrobel et al. 2015, 2016), this regime has only been reached in the Local Group, for M31's G1 with its $M_{\rm IMBH}^{\rm FP} < 10^{3.2}\ M_\odot$ (Miller-Jones et al. 2012).

Each IMBH mass threshold in Figure 4 suffers from a considerable scatter of 0.44 dex. Still, such thresholds do open up the prospect of searching for accretion signatures from IMBHs in tens of GC candidates at a distance of 16.7 Mpc, in the GC-rich Virgo Cluster. Deeper X-ray imaging of NGC 4472, with either Chandra or its possible successor, Lynx, could reveal sources with lower values of $L_{\rm X}^{\rm det}$ in its 698 other GC candidates. Each such new datum added to Figure 4 would have a rightward shift on the abscissa and an upward shift on the ordinate, thereby giving access to a higher $M_{\rm IMBH}^{\rm FP}$ value.

3.5. *IMBH Masses and Bondi Accretion*

This scenario involves predicting the mass of an IMBH that, if accreting at the Bondi rate from the tenuous gas supplied to the GC from its evolving stars, is consistent with the synchrotron radio luminosity of the GC (Maccarone 2004; Strader et al. 2012). Classic Bondi flows involve perfect gases, with spatially infinite distributions, accreting onto isolated central masses, IMBHs in our case. This scenario may be overly simplistic for GC settings but can still offer useful guidance.

Some systematic uncertainties need to be recognized. First, the thermodynamic state – isothermal, adiabatic or intermediate between the two – of the gas flow feeding the Bondi accretion is unknown in GCs. To quantify the importance of this shortcoming, we note that the accretion rate for the isothermal Bondi case is almost a factor of ten higher than for the adiabatic case (e.g., Pellegrini 2005). For a given IMBH mass, the accretion signature from a Bondi flow will thus be stronger for the isothermal case. This led Tremou et al. (2018) to argue that upper limits on accretion signatures yield conservative IMBH mass limits if interpreted within the context of isothermal Bondi flows, rather than even the intermediate Bondi flows assumed earlier (Maccarone et al. 2003; Strader et al. 2012).

However, the study by Pepe & Pellizza (2013) raises a second systematic uncertainty: for four Milky Way GCs that study numerically solved the accretion rates for isothermal Bondi flows toward IMBHs embedded in realistic GC potentials. They reported that the flows appeared to achieve higher accretion rates than classic isothermal Bondi flows. This cautions that IMBH masses inferred from classic isothermal Bondi flows need not be the most conservative values available.

Recent hydrodynamical simulations of gas flows in early-type galaxies favor an adiabatic behavior (Inayoshi et al. 2020), with its lower accretion rates in comparison to the isothermal case (Pellegrini 2005). Future hydrodynamical simulations of gas flows in GCs will eventually establish their true physical properties. In the interim, our aim here is to simply benchmark the accretion signatures. Being mindful of the systematic uncertainties mentioned above, we follow our earlier work on Milky Way GCs (Maccarone 2004; Strader et al. 2012) and extragalactic GCs (Wrobel et al. 2015, 2016, 2018; Wrobel & Nyland 2020), and assume fiducial Bondi flows where the thermodynamic state of the gas is intermediate between the isothermal and adiabatic cases. Specifically, we assume (Strader et al. 2012):

i. For a given IMBH mass $M_{\rm IMBH}^{\rm B}$, gas is captured at 3% of a fiducial Bondi rate for a density of 0.2 particles cm^{-1} (Freire et al. 2001; Abbate et al. 2018) and a temperature of 10^4 K (Scott & Rose 1975). We caution that the density estimate hinges on measurements of only two objects, namely the Milky Way GCs 47 Tuc and M15.

ii. Accretion proceeds at less than 2% of the Eddington rate, thus setting up an inner advection-dominated accretion flow with a predictable, persistent X-ray luminosity $L_{\rm X}^{\rm B}$ (Maccarone 2004).

iii. Given $M_{\rm IMBH}^{\rm B}$ and $L_{\rm X}^{\rm B}$, a radio luminosity $L_{\rm 6cm}$ can be estimated from the empirical fundamental-plane relation. A flat radio spectrum is used to scale from $L_{\rm 6cm}$ to $L_{\rm 2cm}$.

With assumptions $i-iii$, the radio luminosity thresholds $L_{\rm 2cm}$ shown in Figure 2 can be converted to the IMBH mass thresholds $M_{\rm IMBH}^{\rm B}$ displayed in Figure 5, for both individual GC candidates and radio-stacked GC candidates. The statistical uncertainties in the parameters adopted for the conversion cause each IMBH mass threshold to have a statistical error of 0.39 dex (Strader et al. 2012). The fiducial Bondi model suggests access to IMBH masses of $M_{\rm IMBH}^{\rm B} \sim 10^{4.9-5.1}\ M_\odot$ for all 728 individual GC candidates and of $M_{\rm IMBH}^{\rm B,stack} \sim 10^{4.5}\ M_\odot$ for radio stacks of about 100-200 GC candidates (Table 1). Encouragingly, that stack level at a distance of 16.7 Mpc resembles the stack level reported from VLA

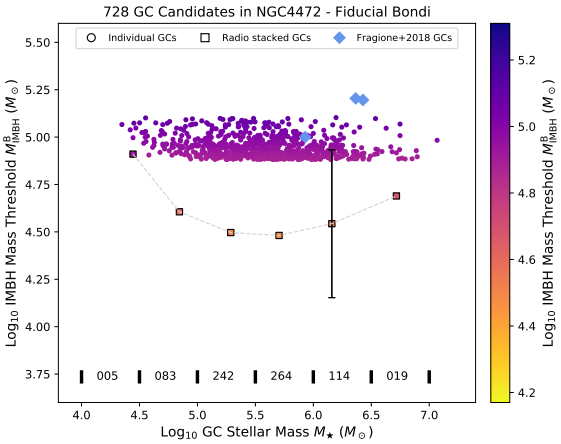

Figure 5. IMBH mass thresholds $M^{\rm B}_{\rm IMBH}$ predicted from a fiducial Bondi accretion model of GC candidates in NGC 4472 (Maccarone et al. 2003), versus the stellar masses $M_\star$ of the GC candidates. The color gradation encodes the IMBH mass thresholds. The circles mark 728 individual GC candidates. Their spread in $M^{\rm B}_{\rm IMBH}$ reflects the spread in $L_{\rm 2cm}$ in Figure 2. The numbers of GC candidates in bins of width 0.5 dex in stellar mass $M_\star$ are noted. The squares mark the IMBH mass thresholds $M^{\rm B,stack}_{\rm IMBH}$ after stacking the GC candidates in each of the bins. The error bar shows the 0.39 dex uncertainty in each IMBH mass threshold, whether individual or stacked. Example predictions from a semi-analytic model for GC evolution over cosmic time are shown (Fragione et al. 2018).

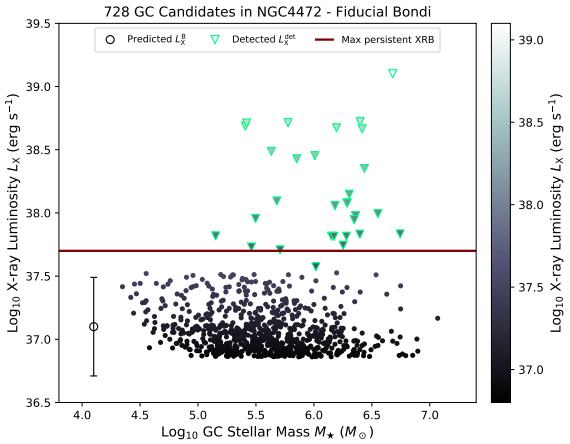

Figure 6. Circles show the X-ray luminosity thresholds $L^{\rm B}_{\rm X}$ predicted from a fiducial Bondi accretion model for 728 GC candidates in NGC 4472 (Maccarone et al. 2003), versus the stellar masses $M_\star$ of the GC candidates. The error bar shows the statistical uncertainty of 0.39 dex in each $L^{\rm B}_{\rm X}$ value, with the spread among values reflecting the spread in $L_{\rm 2cm}$ in Figure 2. The triangles show the X-ray luminosities $L^{\rm det}_{\rm X}$ of the 30 Chandra-detected GC candidates in Figure 3. The color gradation encodes the X-ray luminosities. The horizontal line shows the maximum persistent luminosity of stellar-mass XRBs (Maccarone et al. 2003).

observations of 49 massive GCs in M81 at a distance of 3.6 Mpc (Wrobel et al. 2016).

For context, Fragione et al. (2018) offer three examples of how a star cluster's stellar mass and IMBH mass could evolve to yield a massive, present-day GC. Those examples, plotted in Figure 5, achieve present-day values of $M^{\rm Fra}_\star \sim 10^{5.9-6.4}\ M_\odot$ and $M^{\rm Fra}_{\rm IMBH} \sim 10^{5.0-5.2}\ M_\odot$. At similar stellar masses, the $M^{\rm Fra}_{\rm IMBH}$ values are formally within twice the statistical error on the $M^{\rm B}_{\rm IMBH}$ values, whether for individual GCs or radio-stacked GCs. But this is a weak statement, due to the substantial statistical uncertainties of the fiducial Bondi model as well as to the aforementioned systematic uncertainties.

For the 728 GC candidates, the fiducial Bondi model also yields predictions of $L^{\rm B}_{\rm X}$, the X-ray luminosity thresholds for hard-state emission in the $0.5 - 10$ keV band. These predictions are shown in Figure 6, along with an indication of their statistical uncertainty of 0.39 dex (Strader et al. 2012). The $L^{\rm B}_{\rm X}$ thresholds appear to cluster below the $L^{\rm det}_{\rm X}$ values of the 30 Chandra-detected GC candidates. As discussed in Section 3.2, those 30 X-ray detections could correspond to XRB systems in their high/soft state or very high state, with no relation at all to the presence or absence of accreting IMBHs. But if some of the 30 X-ray detections are hard-state emitters involving accreting IMBHs, Figure 6 suggests that the fiducial Bondi model could be underpredicting their $L^{\rm B}_{\rm X}$ thresholds.

Figure 6 also indicates that the predicted $L^{\rm B}_{\rm X}$ thresholds for all 728 GC candidates appear to cluster below the maximum persistent luminosity of stellar-mass XRBs (Maccarone et al. 2003). While deeper X-ray imaging could reveal additional sources with lower values of $L^{\rm det}_{\rm X}$ in the GC candidates, such imaging on its own would not be able to say if any detections of hard-state X-ray emission arose from stellar-mass XRBs or from fiducial Bondi flows onto IMBHs. This represents a serious X-ray contamination issue, and is the reason why we opted to avoid reporting in Table 1 the X-ray luminosities from the radio-stacked GCs.

We do not mean to discourage deeper X-ray imaging of NGC 4472 with either Chandra or its possible successor, Lynx: such imaging, when combined with ngVLA imaging and a FP analysis, can be used to separate X-ray detections into bins for X-ray binaries and for IMBHs (Wrobel et al. 2018). Also, X-ray binaries are known to be time-variable in both the radio and X-ray bands, so such radio–X-ray synergy would be strengthened by si-

multaneous observations with the ngVLA and the X-ray mission.

4. SUMMARY AND CONCLUSIONS

We simulated a 60-hour observation with the ngVLA of 728 GC candidates in NGC 4472, at a distance of 16.7 Mpc and the optically brightest galaxy in the Virgo Cluster. Interpreting the 2cm detection thresholds as signatures of accretion onto IMBHs, we benchmarked IMBH mass thresholds in three scenarios and found:

1. Radio analogs of ESO 243-49 HLX-1, a strong IMBH candidate with $M_{\rm IMBH}^{\rm HLX} \sim 10^{4-5}\ M_\odot$ in a star cluster, are easy to access in all GC candidates.

2. For the 30 GC candidates with exisitng X-ray detections, the empirical fundamental-plane relation suggested access to $M_{\rm IMBH}^{\rm FP} \sim 10^{1.7-3.6}\ M_\odot$, with an uncertainty of 0.44 dex. Such IMBH levels have been reached only for M31's G1 at a distance of less than 1 Mpc.

3. For all GC candidates and for radio stacks of about 100-200 GC candidates, a fiducal Bondi accretion model suggested access to IMBH masses of $M_{\rm IMBH}^{\rm B} \sim 10^{4.9-5.1}\ M_\odot$ and $M_{\rm IMBH}^{\rm B,stack} \sim 10^{4.5}\ M_\odot$, with uncertainties of 0.39 dex. That IMBH stack level resembles the stack level reported for GCs in M81 at a distance of 3.6 Mpc. Although the fiducial Bondi model offers initial guidance, it should be superceeded by hydrodynamical simulations of gas flows in GCs.

ACKNOWLEDGMENTS

The NRAO is a facility of the National Science Foundation (NSF), operated under cooperative agreement by AUI. The ngVLA is a design and development project of the NSF operated under cooperative agreement by AUI. Basic research in radio astronomy at the U.S. Naval Research Laboratory is supported by 6.1 Base Funding.

Software: astropy (The Astropy Collaboration 2018)

REFERENCES

Abbate, F., Possenti, A., Ridolfi, A., et al. 2018, MNRAS, 481, 627

Anderson, J. & van der Marel, R. P. 2010, ApJ, 710, 1032

Astropy Collaboration, 2018, AJ, 156, 123

Bahramian, A., Strader, J., Miller-Jones, J. C. A., et al. 2020, ApJ, 901, 57

Baumgardt, H. 2017, MNRAS, 464, 2174

Blakeslee, J. P., Jordan, A., Mei, S., et al. 2009, ApJ, 694, 556

Brodie, J. P., & Strader, J. 2006, ARA&A, 44, 193

Cseh, D., Webb, N. A., Godet, O., et al. 2015, MNRAS, 446, 3268

Do, T., Wright, S., Barth, A. J., et al. 2014, AJ, 147, 93

Durrell, P. R., Cote, P., Peng, E. W., et al. 2014, ApJ, 794, 103

Falke, H., Koerding, E., & Markoff, S. 2004, A&A, 414, 895

Farrell, S. A., Webb, N. A., Barret, D., Godet, O., & Rodrigues, J. M. 2009, Nature, 460, 73

Farrell, S. A., Servillat, M., Pforr, J., et al. 2012, ApJ, 747, L13

Fender, R., & Belloni, T. 2012, Science, 337, 540

Fragione, G., Leigh, N. W. C., Ginsburg, I., & Kocsis, B. 2018, ApJ, 867, 119

Freire, P. C., Kramer, M., Lyne, A. G., et al. 2001, ApJL, 557, L105

Godet, O., Plazolles, B., Kawaguchi, T., et al. 2012, ApJ, 752, 34

Greene, J. E., Strader, J., & Ho, L. C. 2020, ARA&A, 58, 257

Gultekin, K., King, A. L., Cackett, E. M., et al. 2019, ApJ, 871, 80

Harris, W. E., Harris, G. L., & Alessi, M. 2013, ApJ, 772, 82

Holley-Bockelmann, K., Gultekin, K., & Shoemaker, D. 2008, ApJ, 686, 829

Inayoshi, K., Ichikawa, K., & Ho, L. C. 2020, ApJ, 894, 141

Jordan, A., McLaughlin, D. E., Cote, P., et al. 2007, ApJS, 171, 101

Jordan, A., Peng, E. W., Blakeslee, J. P., et al. 2009, ApJS, 180, 54

Maccarone, T. J. 2004, MNRAS, 351, 1049

Maccarone, T. J., Kundu, A., & Zepf, S. E. 2003, ApJ, 586, 814

Maccarone, T. J., & Servillat, M. 2008, MNRAS, 389, 379

Maccarone, T. J., & Servillat, M. 2010, MNRAS, 408, 2511

Merloni, A., Heinz, S., & DiMatteo, T. 2003, MNRAS, 345, 1057

Table 1. Stacked GC Candidates in NGC 4472

Stacked Attribute	Bin 1	Bin 2	Bin 3	Bin 4	Bin 5	Bin 6
Number of GC candidates	5	83	242	264	114	19
Median GC Stellar Mass, $\mathrm{Log}_{10}\ M_{\star}^{\mathrm{stack}}$ ($M_{\odot}$)	4.44	4.84	5.29	5.70	6.16	6.72
Flux Density Threshold, $S_{2\mathrm{cm}}^{\mathrm{stack}}$ (μJy beam^{-1})	0.122	0.018	0.009	0.008	0.012	0.031
Radio Luminosity Threshold, $\mathrm{Log}_{10}\ L_{2\mathrm{cm}}^{\mathrm{stack}}$ (erg s^{-1})	32.82	32.00	31.71	31.67	31.83	32.23
IMBH Mass Threshold, Fiducial Bondi, $\mathrm{Log}_{10}\ M_{\mathrm{IMBH}}^{\mathrm{B,stack}}$ ($M_{\odot}$)	4.91	4.61	4.50	4.48	4.54	4.69

Middleton, M. J., Miller-Jones, J. C. A., Markoff, S., et al. 2013, Nature, 493, 187

Miller-Jones, J. C. A., Wrobel, J. M., Sivakoff, G. R., et al. 2012, ApJ, 755, L1

Nagar, N. M., Falcke, H., & Wilson, A. S. 2005, å, 435, 521

Norris, M. A., van de Ven, G., Kannappan, S. J., Schinnerer, E., & Leaman, R. 2019, MNRAS, 488, 5400

Nyland, K., Young, L. M., Wrobel, J. M., et al. 2016, MNRAS, 458, 2221

Nyland, K., Harwood, J. J., Mukherjee, D., et al. 2018, ApJ, 859, 23

Pellegrini, S. 2005, apj, 624, 155

Pepe, C., & Pellizza, L. J. 2013, MNRAS, 430, 2789

Plotkin, R. M., Markoff, S., Kelly, B. C., Koerding, E., & Anderson, S. F. 2012, MNRAS, 419, 267

Rui, Z., Weatherford, N. C., Kremer, K., et al. 2021, Res. Notes, 5, 47

Scott, E. H., & Rose, W. K. 1975, ApJ, 197, 147

Selina, R. J., et al. 2018, in ASP Conf. Ser. 517, Science with a Next Generation Very Large Array, ed. E. J. Murphy et al. (San Francisco, CA: ASP), 15

Soria, R., Hakala, P. J., Hau, G. K. T., et al. 2012, MNRAS, 420, 3599

Soria, R., Musaeva, A., Wu, K., et al. 2017, MNRAS, 469, 886

Strader, J., Chomiuk, L., Maccarone, T. J., et al. 2012, ApJL, 750, L27

Tremou, E., Strader, J., Chomiuk, L., et al. 2018, ApJ, 862, 16

van der Marel, R. P. & Anderson, J. 2010, ApJ, 710, 1063

Willmer, C. N. A. 2018, ApJS, 236, 47

Wilman, R. J., Miller, L., Jarvis, M. J., et al. 2008, MNRAS, 388, 1335

Wrobel, J. M., Nyland, K. E., & Miller-Jones, J. C. A. 2015, AJ, 150, 120

Wrobel, J. M., Miller-Jones, J. C. A., & Middleton, M. J. 2016, AJ, 152, 22

Wrobel, J. M., Wrobel, J. M., Miller-Jones, J. C. A., Nyland, K. E., & Maccarone, T. J. 2018, in ASP Conf. Ser. 517, Science with a Next Generation Very Large Array, ed. E. J. Murphy et al. (San Francisco, CA: ASP), 743

Wrobel, J. M., & Nyland, K. E. 2020, ApJ, 900, 134